EFFICIENT SEPARATION OF HEAVY METALS BY ANCHORING POLYMER COMPOSITE PVA/PVP/BENTONITE ON SUPERPARAMAGNETIC MAGNETITE NANOPARTICLES THROUGH SURFACE MODIFICATION

Abdulhady, Yasser A.M.
Water Treatment and Desalination Unit, Department of Hydrogeochemistry, Desert Research Center, Cairo, Egypt
E-mail: yasser_vip6@hotmail.com

The present research work has been carried out to assess the efficiency of nanocomposite bentonite/Fe_XO_y, coated by polyvinyl alcohol (PVP/poviden PVP), in the absorption of cation pollutants. Chemical treatment was proved by using nanocomposite bentonite/Fe_xO_y coated by polyvinyl alcohol (PVA/povidone PVP). Purified local bentonite in nano-sized model was synthesized by co-precipitation process. X-ray diffraction analysis (XRD) and other techniques have been used for the characterization of the prepared materials. The mean diameter of nanocomposite material sizes was around 31.5 nm. The presence of functional groups of polymer around a core of nano-Fe_xO_y has been confirmed. Magnetic measurements have been made with a vibrating sample magnetometer (VSM), which demonstrate the superparamagnetic nature of the nanocomposite with higher saturation magnetization, but when bentonite merged with nano-magnetite new data have been given showing relatively lower saturation magnetization than before. The purpose of work is to explain the valuability of bentonite/PVA-PVP/Fe_XO_y for adsorption of cations pollutant and its efficiency by graft polymerization of modified bentonite IONPs. The removal efficiency of five heavy metals Co, Cr, Cu, Fe, and Mn was 83.40%, 84.66%, 86.50%, 90.06% and 85.66%, respectively. Optimal conditions of nanocomposite bentonite/PVA-PVP/Fe_XO_y experiment were nanocomposite dosage at 7.5 g/L; contact time at 30 min; temperature at 50^{o}C and pH at 6.0.

Keywords: nanocomposite bentonite/Fe_xO_y, polyvinyl alcohol (PVA/povidone PVP), adsorption, heavy metals

INTRODUCTION

Modified bentonite is applied in many implementations such as adsorbents of different pollutants of soil and water paints components in the preparation of clay coated by poly vinyl group (Betega et al., 2008 and He et al., 2010). Preparation of clays is depended on mechanism that clay minerals have with different silicates and aluminates groups with varies hydroxyl groups as active site. Substitution reactions occur by displacing H_2O inside space structure of bentonite by polar skeleton. Some organic structures form complexes with interlayer cations. Hydrogen bonds, coordination bonds, neutralized reactions, and van der Waals forces. In the case of bentonite, the adsorption occurs on chemical reaction in clay actions. Varies synthesized methods such as co-precipitation (Petcharoen et al., 2012), hydrothermal (Li et al., 2015), thermal decomposition (Sharma and Jeevanandam, 2013), microemulsion (Okoli et al., 2012) electrochemical deposition (Karimzadeh et al., 2017), laser pyrolysis (Morjan et al., 2010), solvothermal methods (Ooi et al., 2015), sonochemical methods (Abbas et al., 2013), chemical vapor deposition (Wang et al., 2015), the microwave assisted method (Solano et al., 2012), and aerosol pyrolysis (Strobel and Pratsinis, 2007) have been reported to prepare MIONPs. Bentonite has an aluminates and silicate structures with varied layers. Bentonite has two four-dimensional coats and one eight-dimensional coat. Moreover, nano bentonite/PVA-PVP/Fe_XO_y has been applied as water purified factor due to their highly magnetism cases, high surface area, simple methodology, non-toxicity, and proper bioavailability (Karnland et al., 2006 and Murray, 2006). In addition, Fe_XO_y magnetic nanoparticles obtain on varies groups like OH and acid groups. Therefore, these matters would have various applications for the link of compounds in water and wastewater industry.

Nanotechnology has large, interesting research band in future due to having more applications. Fe_XO_y is a vital magnetic structure that has good biocompatibility character and super-paramagnetic type in nano-sized diameters (Catalano et al., 2017). Magnetic strength of Fe_XO_y is responsible to attach with different polluting cations (Moise et al., 2017). In addition, magnetite has an ability to compact with energy of magnetic lines into thermo or mechanical support. It used in medical field like magnetic hyperthermia (Sunaryono et al., 2016). Addition to materials was preventing to get excellent effeminacy (Zustiak and Leach, 2010). Several polymers were added which have biodegradable and biocompatibility features (de Mello et al., 2019). Fe_XO_y used as filler matters such as the magnetic hydrogel. Ferrogels are complex that used in biomedical as magneto sensitive transformers (Kurlyandskaya et al., 2017). Ferrogel is prepared by two different matters a as example magnetic nanomaterials filler and hydrogel polymer (Hidayat et al., 2019). More research used different types of polymer as support in ferrogel

of synthesis such as PVA (Sunaryono et al., 2018), polyacrylamide (Safronov et al., 2018), gelatin (Wisotzki et al., 2016), (PVP/PVA) polymers do as aid materials in ferromagnetic gel structure. The PVP and PVA polymers have definite properties for ferrogel such as non-toxic, inexpensive, and simple preparation methods (Lu et al., 2012; Gonzalez et al., 2014 and Shi et al., 2016). These advantages of PVP/PVA get using as good materials for ferrogel (Adriane et al., 2006). Ferrogels consists of nano-magnetic materials, but hydrogel polymers have mobility to attract on the external magnetic field. Ferrogels have some kinetics properties if these materials interact to thermal activation by the induction of an external magnetic field (Brazel, 2009). The ferrogel in nano-sized formed from varies polymer hydrogel. Crystal's diameter is 3.9 nm and distributed with the distance between them by 18 nm. The crystallite diameter was about 2.8-3.3 nm with the distance between crystallites of 15-17.5 nm (Zhang et al., 2016). In this work, we report the success fabrication of modified bentonite/IONPs with PVA/PVP based on ferrogel. The co-precipitation method is the main chemical processes to get on nanocomposite of bentonite-Fe_xO_y in nanoscale. This modified nanocomposite can be recommended to be used remove different pollutants in wastewater. The reduction percentage of synthesized nanocomposite with heavy metals and some other pollutants has given high results. The usage of local Egyptian bentonite in this work gave a new chemical feature in nanocomposite and make wastewater treatment with high quality and economic feasibility. The new modification of bentonite graft polymerization with hydrogel and magnetic nanoparticles were investigated.

MATERIALS AND METHODS

Ferric chloride hexahydrate ($FeCl_3.6H_2O$), ferrous chloride tetra-hydrate ($FeCl_2.4H_2O$) and ammonium hydroxide (NH_4OH) & NaOH & HCl and nitric acid and ethyl alcohol/ acetone were purchased from Merck. Natural bentonite was obtained from local supplier. Samples were collected from Municipal plant with sterilized bottles covered with ice cubes and kept at 4°C for analyzing the various parameters. Poly-vinyl-alcohol and polyvinylpyrrolidone with an average molecular weight of 93,000 g/mol and a hydrolysis degree higher than 98–99% were purchased from Sigma-Aldrich Company.

1. Procedure of Clay Purification

The first method is purification of local Egyptian clay mineral by acidification. In our study, 100 g of raw clay several HCl concentrations were added to remove excess of carbonate mainly and other several oxides and hydroxyl compounds. Modified suspensions were stirred for 2 h at a room temperature and afterwards decanted. The second step was preparation of iron oxide from merging of ferrous and ferric inorganic salts prior to the reaction with NH_4OH and its amount was adjusted to obtain the bentonite/PVA-

PVP/Fe_XO_y oxide weight ratios of 3:1 and 6:1 with vigorous stirring with purified clay. Concentrated alkai was added to the solution to get new nanocomposite. Solution was washed by DEM water numerous times, and then dried at a temperature of 105°C.

2. Methodology of Bentonite Coated on IONPs (bentonite/PVA-PVP/Fe_XO_y)

The planning of modified silicates coated depended on the method of Bourlinos et al. (2000). A weight of 10 g of bentonite was steeped in 500 ml of condensate H_2O, 200 ml of 0.02 M $FeCl_2 \cdot 4H_2O/FeCl_3.6H_2O$ and 150 ml of hydrogel emulsion PVA/PVP was added with ratio of 6:1 (pH at 3.5 by sodium hydroxide) and gathered with stirring. The suspension was centrifuged and washed extra times by H_2O for 30 min. This procedure was repeated for two times like before. The new sediment was diffused and dried at room temperature. The layer produced was bared to excess glacial CH_3COOH vapors for 2 h at 80°C, crushed into powder and calcined at 400°C for 3 h to get nanocomposite (Hong et al., 2006 and Indira and Lakshmi, 2012). The function of surfactants (also referred here as ligands) like stearate compounds were bound to the surface of the nanocrystals and increased a steric hindrance and aggregation.

3. Characterization of Modified Nanocomposite

3.1. Sample instrumentation

The x-ray diffraction analysis (XRD) item of nanocomposite bentonite-Fe_XO_y was getting by a X-ray diffractometer Schimadzu model. Magnetization of nanocomposite was evaluated by the collection of magnetic particles. Coercively, remanence and saturation of samples have been evaluated. FT-IR spectroscopy was magnitude in a transmission mode on a spectrophotometer (PerkinElmer Spectrum Version 10.03.09) Spectrum Two Detector $LiTaO_3$. The samples were put into pellets of a mixture with KBr. SEM Model Quanta 250 FEG (Field Emission Gun) was used for determining the shape of nanoparticles surfaces. Concentrations of trace metal ions were detected by ICP-AMS, Optima 3000XL, Perkin Elmer.

3.2. Detecting nano-composite power

The adsorption techniques were played through blending nanocomposite bentonite/IONPs with 100 ml of the synthesized samples. Using 0.1M HCl and 0.1M NaOH solutions to modify pH. Nanocomposite mixture/wastewater solution was put in a sonicator. Hydrogel nanocomposite bentonite/IONPs was washed by DEM.

3.3 Batch adsorption experiments

Adsorption % was measured through this equation.

$$\% \text{ Removal} = (C_i - C_f) / C_i * 100 \quad (1)$$

C_f and C_i are the initial and final concentration of pollutants, respectively.

Adsorption capacity

$$q_e = (C_0\text{-}C_e)\ V/M \qquad (2)$$

qe / Adsorption capacity

C_0 and C_e are initial and balanced concentrations (mg/L)

V / volume of the solution (L)

M / The amount of used adsorption (g)

3.4. Isotherm studies

The adsorption isotherm models were investigated as detecting a maximum capacity of an adsorbent and explaining the mechanism of adsorption. The prepared magnetic nanocomposite was shacked for 30 min at room temperature and in a water bath, 15 mg of solute with several 100 ml pollutant ions; ranged from 25 to 200 mg/L at pH 7. Nanocomposite was disconnected and of Fe and Mn ions concentration was determined by the aforementioned method. Langmuir and Freundlich isotherm were explained to investigate the reaction mechanism. Langmuir model shows mono-coat adsorption at homo connection on the adsorbent face (Choe et al., 2000). Freundlich model backup multi-layer of adsorbate onto hetero face of the adsorbent (Huang and Zhang, 2002).

3.5. Kinetic techniques

Kinetic models were evaluated the adsorption process. The experiment part was performed as follows: The prepared magnetic nanocomposite was shaked, for 30 min at room temperature and in a water bath, 15 mg of solute with several 100 ml pollutant ions; ranged from 25 to 200 mg/L at pH 7. Nanocomposite was disconnected and of Fe and Mn ions concentration was determined by the aforementioned method.

3.6. Thermodynamic techniques

The thermodynamic of an adsorption process is generally detected from the numerical values of three thermodynamic parameters, Gibbs free energy (ΔG^o), standard entropy change (ΔS^o) and standard enthalpy change (ΔH^o). All materials and techniques are illustrated in Fig. (1).

RESULTS AND DISCUSSION

1. Assessment of Acidification Before and After Treatment

Table (1) and Fig. (2) show the chemical composition of different oxide compounds connected with each other by tetragonal and octagonal structures as in bentonite. The silicate compound is considered as a central part of varies structures. Different crystallographic shapes of bentonite contribute in increasing the surface area, which takes part in the removal of several pollutants. Acidification technique for mineral clay purification was the simplest and cheapest chemical method. It is revising mainly on different concentrations of HCl to remove varies soluble chloride salts after treatment to get on purified phase of bentonite.

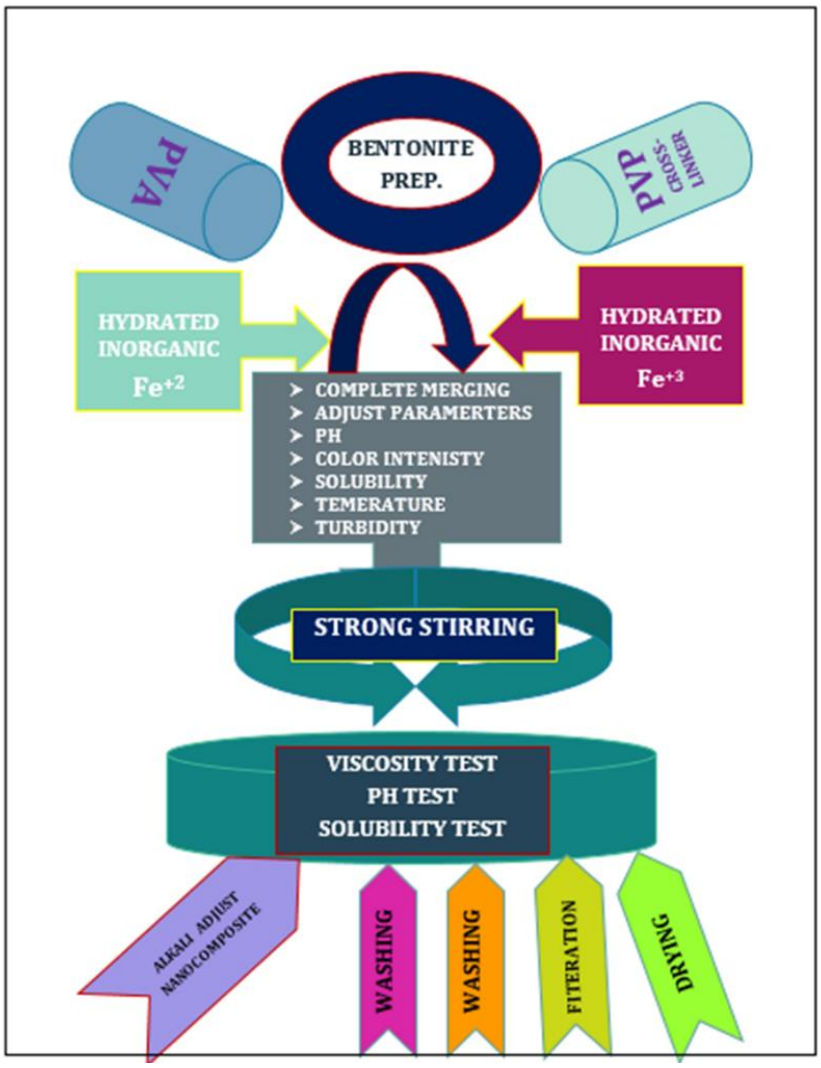

Fig. (1). Schematic of chemical steps of bentonite-Fe_xO_y methodology.

Table (1). Chemical constituents of bentonite before and after acidified purification by x-ray fluorescence.

Composition %	SiO_2	Al_2O_3	Fe_2O_3	CaO	MgO	K_2O	Na_2O	Others
Natural bentonite	61.28	17.79	3.01	4.54	2.10	1.24	2.70	7.30
Treated bentonite	53.80	11.40	23.50	0.47	0.83	1.00	0.60	8.40

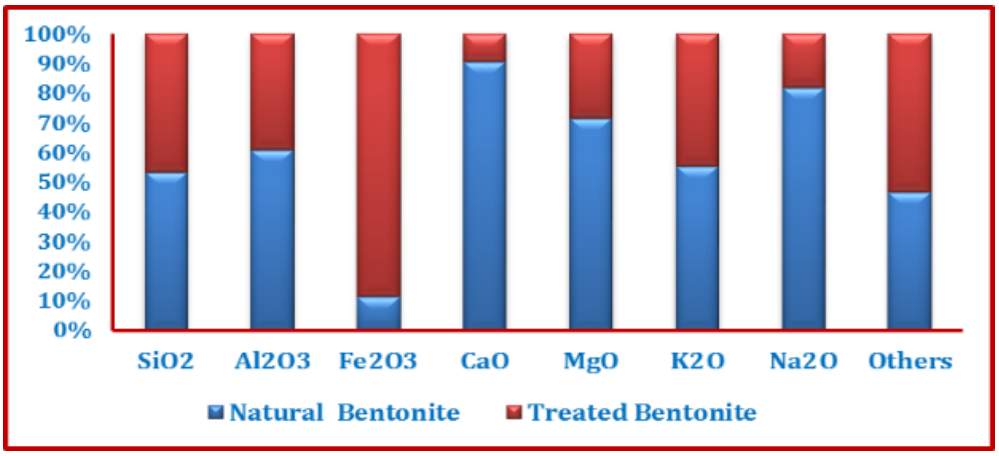

Fig. (2). Chemical composition of bentonite before and after acidified purification by x-ray fluorescence.

2. Mechanism of Nanocomposite Bentonite/PVA-PVP/Fe_xO_y

A purified mixture of bentonite with PVA/PVP was added to Fe^{+2} and Fe^{+3} ions solution with strong stirring at 200 ppm at temperature up to 40–50℃ to get on homogenous solution. Liquid NH_4OH/ NaOH was added dropwise to the solution to get on IONPs ppt. The Fe^{+3} ions reacted with ammonia to give FeOOH. With heating, the reaction gave Fe^{2+} and OH^- ions, and produced finally Fe_3O_4 ions. The nanocomposite mixture has larger surface area than individual nanoparticles (Cornell and Schwertmann, 2003).

3. Characterization of the Bentonite/PVA-PVP/Fe_XO_y

3.1. Evaluation of x-ray diffraction analysis (XRD)

Fig. (3) shows the different sharp peaks intensity at 2 theta 16.50, 21.50, 31.50, 32.50, 43.00, 58.50. The band shifted to the partially crystalline nature of PVA polymer molecules. The PVP band showed broad diffraction peaks around $2\theta = 21.50$. The amorphous shape of polymer had a lowest one. The positions and relative intensities of the reflection peak of Fe_3O_4 and Fe_2O_3 were shown with XRD spectrum. The peak of PVP appeared on 16.50 according to standard peak intensity of PVP. Broad peaks were shown at 43.00 related to magnetite in nano-sized and appear peaks on 2 theta 31.50 for hematite particles which contained by oxidation of magnetite. At 2 theta peak intensity at 58.50 formed a new nanocomposite of bentonite-Fe_XO_y. Appearing of this peak indicated that nanocomposite formation was synthesized with high efficiency and new crystallographic shapes were formed (Mahdavi et al., 2007). The band of crystalline nature of PVA polymer molecules was edited.

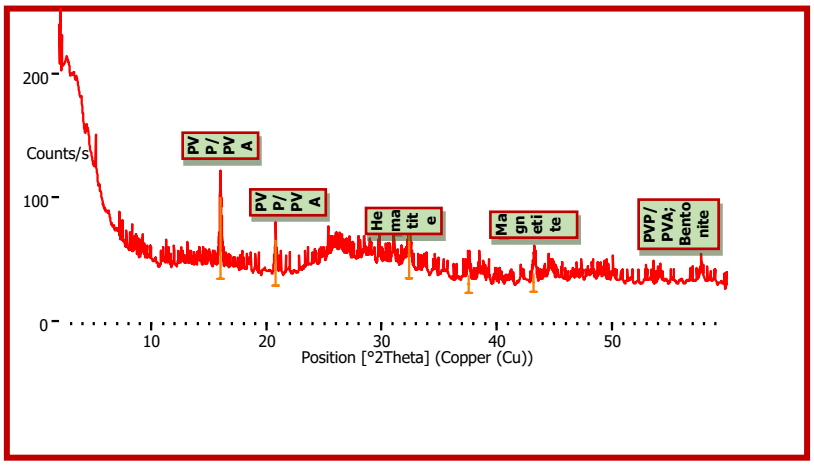

Fig. (3). XRD pattern of bentonite-Fe_xO_y formed.

3.2. Scanning electron microscope (SEM) of bentonite/PVA-PVP/Fe_xO_y

Fig. (4) shows that surface area of nanocomposite bentonite/PVA-PVP/Fe_XO_y, which agrees to cubic and spherical shape of nanocomposite IONPs bentonite/PVA-PVP/Fe_XO_y grafted in bending shape. The SEM illustrated the effective iron inorganic salts to contain nano-core with vary items. By using a mixture of inorganic salts, it gave spherical nanoparticles with large face area. SEM showed the big face area of nanocomposite bentonite-Fe_XO_y with active surface sites that adsorption process took place (Tsukasa, 2017).

3.3. FT-IR spectroscopy of bentonite/PVA-PVP/Fe_xO_y

Fig. (5) shows absorption peaks at 501 cm^{-1} and 479 cm^{-1} showing the Fe–O vibration related to the iron oxide in nano-sized and two absorption peaks at 2,233 and 2,217 cm^{-1} were attributed to the asymmetric C-H stretching and the symmetric C-H stretching, respectively. The aliphatic C–H stretching, in 1416 cm^{-1} were due to C–H bending vibrations. The sharp band at 531-599 cm^{-1} was likely due to the vibration of the Si–O bonds. The IR band at 3405 cm^{-1} could be assigned to the stretching modes of surface H_2O molecules or to an envelope of hydrogen-bonded surface OH groups. Specifically, 667 and 1009 cm^{-1} bands assigned to the bending of silica relation and vibration of silica-alumina. Absorption peak at 1401 cm^{-1} showed the stretching of silica. The band at 3405 cm^{-1} explained to water molecule inside silica-alumina frame. A change of absorption intensity was indicted of the associated differences between the compared structures. The main IR bands were as follows: 1130–1035 cm^{-1} related to Si-O and asymmetrical stretch 1109 cm^{-1} showed to Al-O. Symmetrical stretch (501–593 cm^{-1}) bend to Si-O-Al. The double ring (413-473 cm^{-1}) vibrations related to the interaction between Si-O-Al. Sharp peak appears at 873 cm^{-1} indicated to new linkage asymmetrical stretching band of Si-O-Fe/Al-O-Fe (Shalaby et al.,

2018). IR spectroscopy is consumed to describe minerals as adsorbate systems. Hydration and dehydration of water might be easily observed by IR, since adsorbed H_2O gave increase to a typical deformation band around 1416 cm^{-1}.

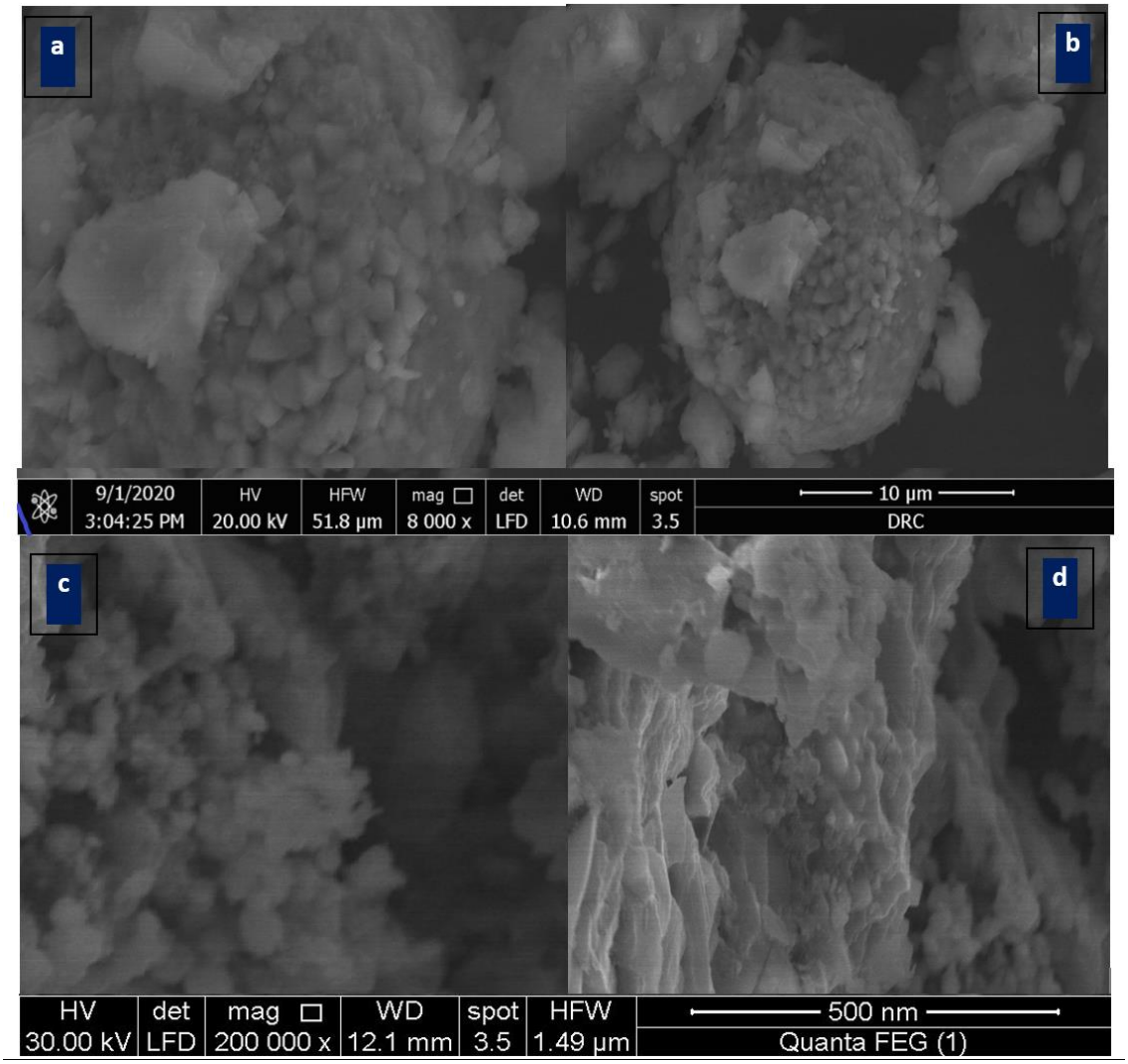

Fig. (4). Scanning electron microscope photos of bentonite/PVA-PVP/Fe_xO_y.

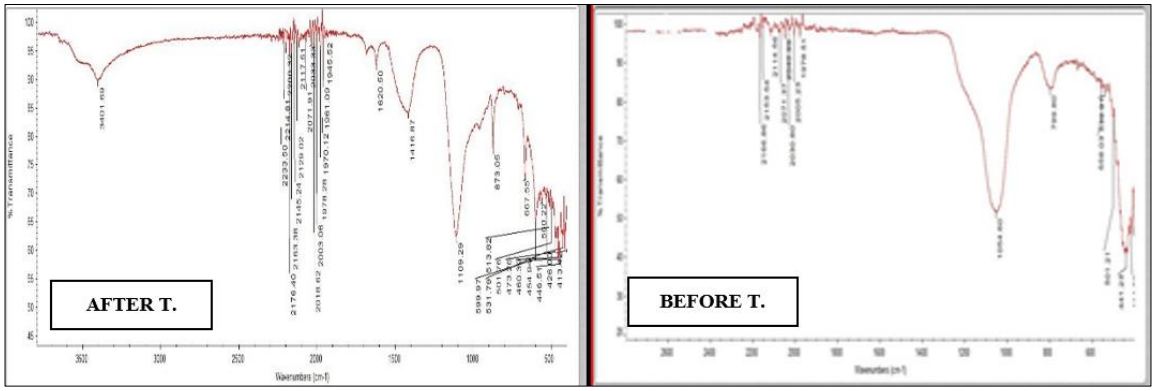

Fig. (5). FT-IR-spectroscopy of nanocomposite before and after treatment.

3.4. Magnetic characterization of nanocomposite bentonite/PVA-PVP/Fe_xO_y (VSM)

Vibrating sample magnetometer (VSM) will help to know magnetic characterization of synthesized nanocomposite. The low hysteresis in the magnetization explained that resulted nanoparticles had paramagnetic strength. The magnetization saturation (MS) data of Fe_xO_y, bentonite and bentonite/PVA-PVP/Fe_xO_y were 35.485 emu/g, 5.413 emu/g and 0.6478 emu/g, respectively. Table (2) and Fig. (6) show that IONPs had high MS values than others. The reading value of MS bentonite has small result (Guo et al., 2010).

Table (2). VSM measurements values for nanocomposite bentonite/PVA-PVP/Fe_xO_y

Parameters	**Fe_xO_y**	**Bentonite**	**bentonite/PVA-PVP/Fe_XO_y**
Coercivity (Hci)	250.41 G	569.21 G	623.80 G
Magnetization (Ms)	35.4850 emu/g	8.38813 emu/g	0.6478 emu/g
Retentivity (Mr)	5.8590 emu/g	0.2410 emu/g	0.19735 emu/g

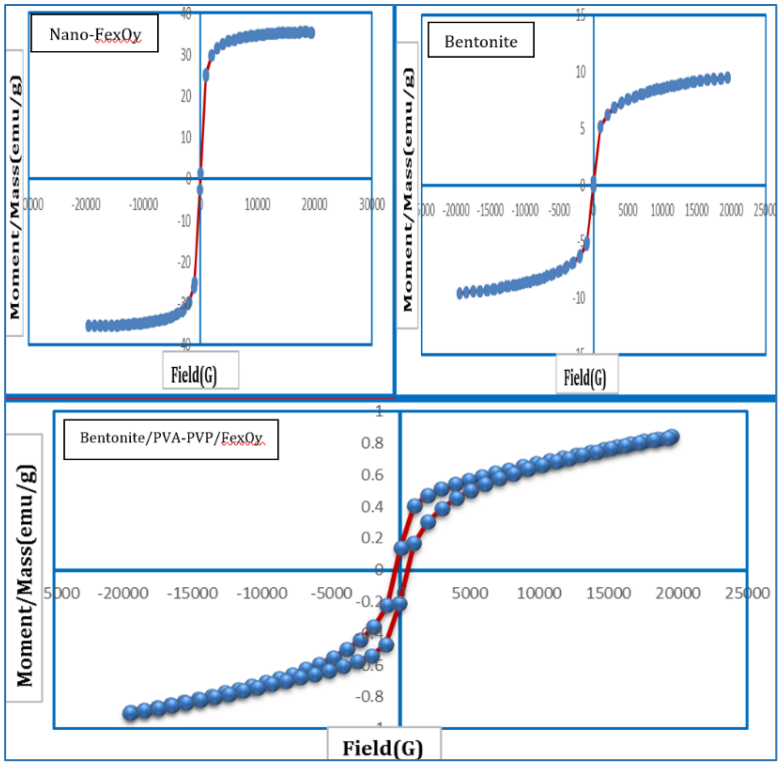

Fig. (6). VSM charts of nanocomposite bentonite/PVA-PVP/Fe_XO_y; nano-Fe_xO_y and bentonite.

3.5. Particle size analysis of nanocomposite bentonite/PVA-PVP/Fe_XO_y

Fig. (7) shows that the average particle size of the nanocomposite compound under consideration have a sphere and crystalline shape. The nanoparticles intensity, volume and number weighting are 48.5 nm, 22.9 nm and 14.5 nm, respectively. The average diameter of nanocomposite was around 31.5 nm. This means that inhibition percentage of prepared bentonite/PVA-PVP/Fe_XO_y related to the size and shape. The particle size distribution test depended mainly on the increase of face area and the removal capability.

4. Adsorption Study of Different Heavy Metals Adsorption on Nanocomposite Bentonite/PVA-PVP/Fe_xO_y for Removal of Wastewater Heavy Metals

4.1. Influence of initial pH

The pH performs an active role in the clearance of pollutants from wastewater. The pH was regulated to the required pH using the best value of nanocomposite bentonite/PVA-PVP/Fe_xO_y dosage of 8 g/L (Table 3 and Fig. 8).

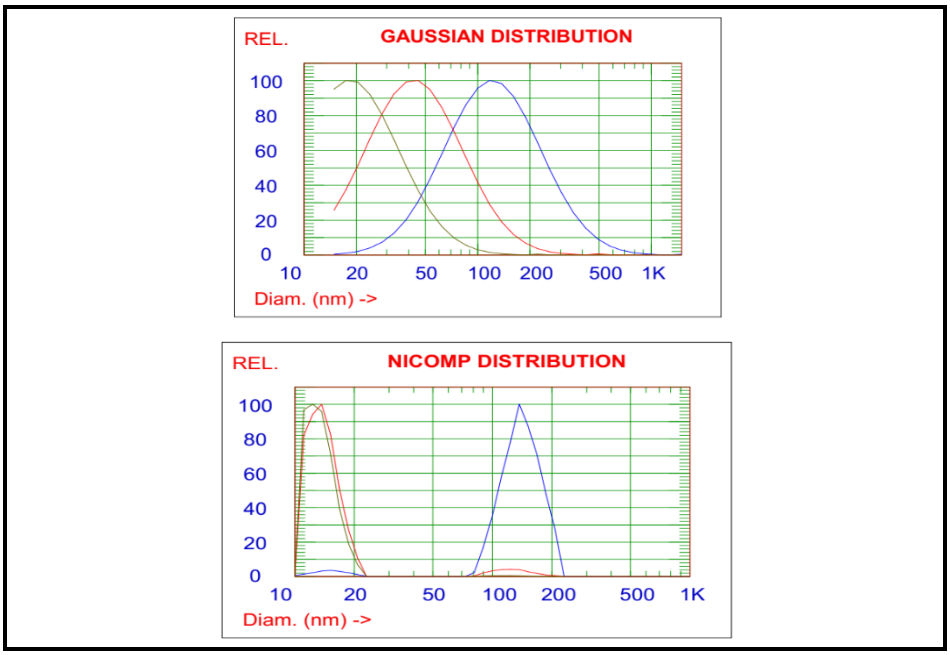

Fig. (7). Particle size distribution (nano-sized) of nanocomposite bentonite/PVA-PVP/Fe_xO_y.

Table (3). Relation between pH and reduction percentage of different polluted heavy metals.

pH	Reduction %				
	Cobalt	**Chromium**	**Copper**	**Iron**	**Manganese**
3	57	64	54	50	41
4	65	76	61	67	55
5	81	86	80	82	70
6	87	90	83	74	83
7	77	81	76	63	72
8	72	77	73	58	68

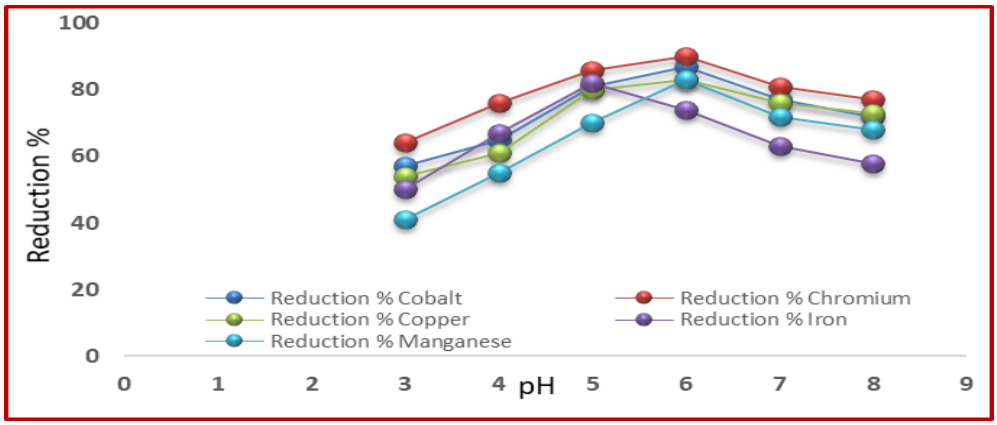

Fig. (8). Influence of pH on the removal of Co, Cr, Cu, Fe and Mn bentonite/PVA-PVP/Fe_xO_y nanocomposite. Dose 8 g/L, contact time 45 min; temp. 50°C.

4.2. Influence of nanocomposite dose

The illuminate of COD, BOD, TOC, TSS, TN and TP with montmorillonite and zeolite/IONPs nanocomposite doses was determined, by using different concentrations of nanocomposite from 2 to 10 g/L as shown in Table (4) and Fig. (9). The montmorillonite and zeolite/IONPs nanocomposite efficiency rose with increasing amounts up to 5 g/L, after that the montmorillonite and zeolite/IONPs nanocomposite efficiency declined with increasing doses. At the optimal montmorillonite and zeolite/IONPs nanocomposite dose (5 g/L), the illumination of COD, BOD, TOC, TSS, TN and TP were 81%, 92%, 86%, 80%, 73% and 75%, respectively. The increase of the nanocomposite efficiency with increasing nanocomposite doses was obtained probably due to the increase of positive charged metal ions concentration to neutralize negative charge organic particles. A head of the optimal nanocomposite doses, the reversal charge took place on the surface of the nanocomposite particles with the excess amount of nanocomposite doses, and hence the decline of the increase of nanocomposite efficiency.

Table (4). The relation between nanocomposite doses and reduction percentage of polluted heavy metals.

Doses (g/L)	Reduction %				
	Cobalt	Chromium	Copper	Iron	Manganese
2	60	62	54	54	49
3	67	70	65	66	62
4	80	81	77	84	70
5	86	84	86	76	83
8	88	86	89	81	87
10	75	75	72	66	78

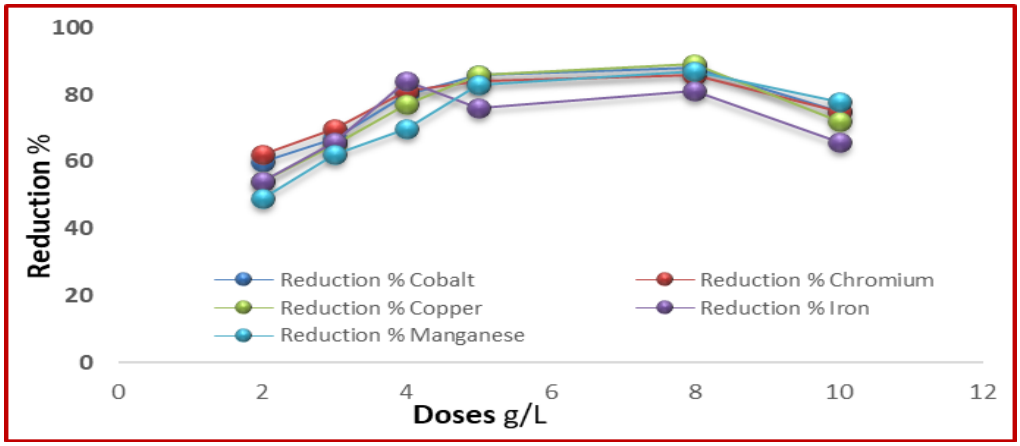

Fig. (9). Influence of nanocomposite doses on the removal of Co, Cr, Cu, Fe and Mn bentonite/PVA-PVP/Fe_xO_y nanocomposite. pH 6; contact time 45 min; temperature at 50°C.

4.3. Effect of contact time on nanocomposite with different pollutants

The contact time plays an important role on the uptake of several pollutants from samples. The effect of nanocomposite ability for reducing COD, BOD, TOC, TSS, TN and TP were determined, as presented in Table (5) and Fig. (10). The removal of COD, BOD, TOC, TSS, TN and TP rose with time, up to 60 min. The reduction percentage increased for COD, BOD, TOC, TSS, TN and TP p to 82%, 88%, 81%, 83%, 81%, and 84%, respectively at the 60 min treatment time.

Table (5). Relation between contact time and reduction percentage of polluted heavy metals.

Contact (time/min)	Reduction %				
	Cobalt	Chromium	Copper	Iron	Manganese
5	45	47	41	38	50
15	59	65	48	49	63
30	70	79	58	65	77
45	87	84	76	80	82
60	80	81	70	75	76
75	73	73	63	70	71

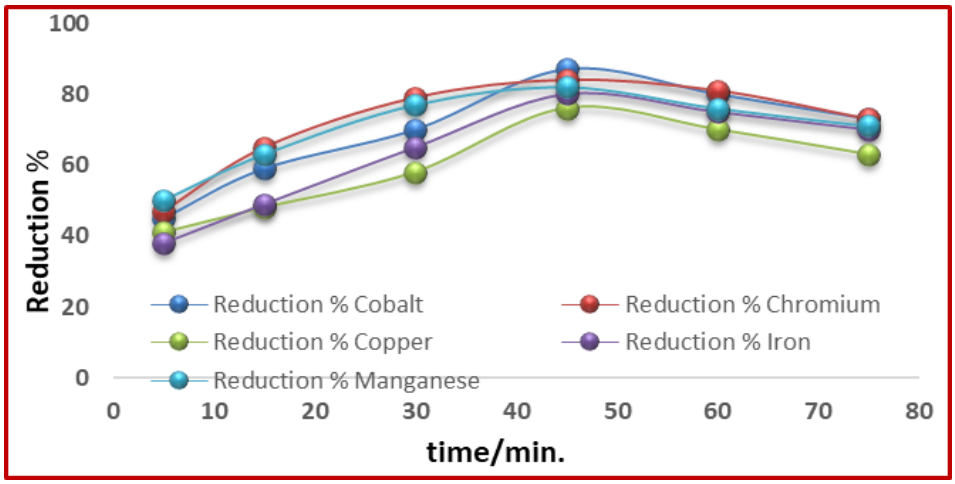

Fig. (10). Influence of contact time on the removal of Co, Cr, Cu, Fe and Mn bentonite/PVA-PVP/Fe_xO_y nanocomposite. pH 6; 8 g/L dose; temperature at 50℃.

4.4. Effect of contact time on montmorillonite and zeolite/IONPs nanocomposite with different pollutants

The removal of COD, BOD, TOC, TSS, TN and TP using nanocomposite was determined with different temperatures 40±1°C to 80°C as shown in Table (6) and Fig. (11). The reducing pollution of COD, BOD, TOC, TSS, TN and TP rapidly would rise with increasing temperature and reached to 60°C. However, the reduction percentage was decreased with the increase of temperature above 60°C. The maximum illumination of pollutants was gained at 70°C. The nanocomposite percentage increased with rising temperature because of the reduction of viscosity with dispersants of the organic compounds.

Table (6). The relations between temperature (℃) and reduction percentage of different pollutants.

Temperature (℃)	Reduction %				
	Cobalt	Chromium	Copper	Iron	Manganese
40	78	78	74	75	77
50	89	90	88	84	87
60	86	87	79	82	80
70	84	81	76	78	73
80	80	80	71	70	71

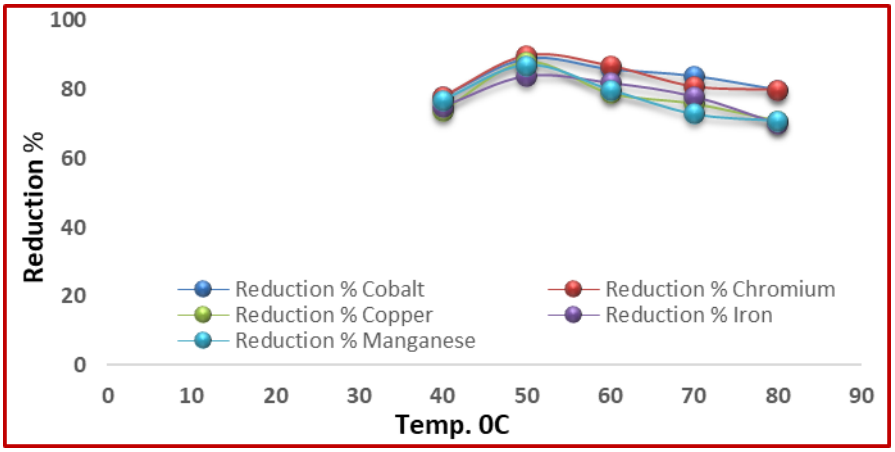

Fig. (11). Influence of temperature on the removal of Co, Cr, Cu, Fe and Mn bentonite/PVA-PVP/Fe_xO_y nanocomposite. pH 6; 8 g/L dose; contact time 45 min.

5. Effect of Bentonite/PVA-PVP/Fe_xO_y on Removal of Wastewater Heavy Metals

Table (7) and Fig. (12) Shows the heavy metals of wastewater samples that have impermissible limit. Cobalt, chromium, copper, iron and manganese elements are considered as most toxic metals in wastewater plant. These elements have chemical activities and abilities to interact with different organic and inorganic compounds through various bonding. So, this study concerned with the synthesis of nanocomposite that have specific chemical adsorption characterization. Nanocomposite bentonite/PVA-PVP/Fe_XO_y could achieve excellent reduction percentage results where these materials have specific surface area and also specific crystallographic shape. also shows the values of heavy metals removal percentage. In cobalt ion, the value of reduction percentage gave 83.66%, chromium ion gave 84.84%, copper gave 83.25%, iron gave 88.49 and the best value with manganese ion was 91.05%.

Table (7). Effect of bentonite/PVA-PVP/Fe_XO_y on heavy metals removal from wastewater samples.

Parameter (mg/L)	Permissible limit [42]	Present study* ±SD	Conc. before treatment	Conc. after treatment	Reduction %
Cobalt	<0.05	0.14±0.01	3.440	0.562	83.66
Chromium	<0.05	0.19±0.08	5.740	0.870	84.84
Copper	<0. 5	0.86±0.01	4.120	0.690	83.25
Iron	<0.3	3.55±0.50	8.460	0.973	88.49
Manganese	<0.5	0.17±0.10S	2.950	0.264	91.05

Optimal conditions; nanocomposite dosage: 7.5 g/L; contact time: 30 min.; temperature: 50°C; pH: 6.0 *All values are in mg/L, samples collected from four diffident sources and were analyzed in triplicates.

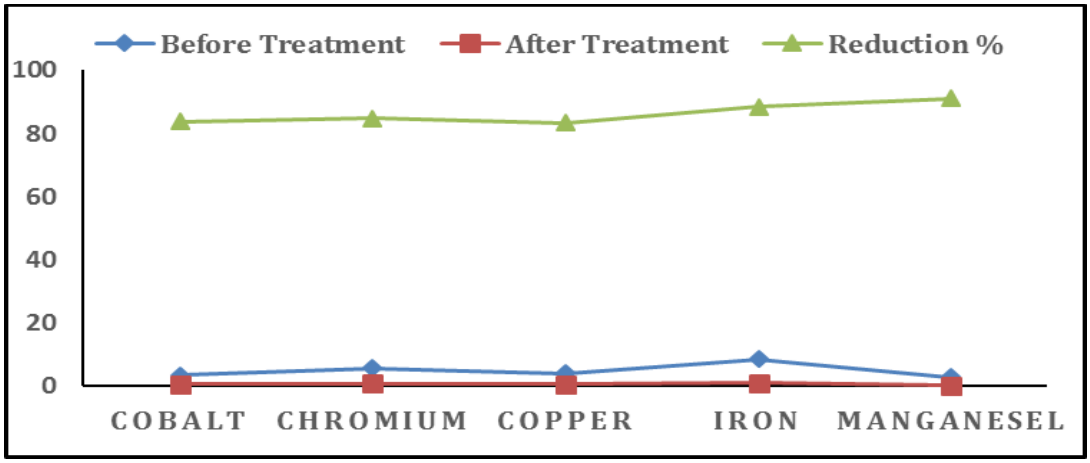

Fig. (12). Treatment before and after five toxic metals by nanocomposite bentonite/PVA-PVP/Fe_xO_y.

5.1. Effect of different concentrations of synthesized polluted cobalt ion on reduction % at optimal conditions of nanocomposite bentonite/PVA-PVP/Fe_XO_y

Table (8) and Fig. (13) show the effect of different concentrations of cobalt on removal efficiency percentage. The highest value of reduction percentage of cobalt was 83.40% at 50 mg/L. After this value the reduction percentage decreased. This is due to minimizing the adsorption capacity of functional groups on nanocomposite bentonite/PVA-PVP/Fe_XO_y surface sites. And the effect of different concentrations of chromium ion on the reduction percentage. The highest removal percentage value of chromium was 84.66% at 30 mg/L. After this value, the reduction percentage decreased because of fully adsorption capacity on active sites of nanocomposite bentonite/PVA-PVP/Fe_XO_y. Table (8) also shows the effect of different concentrations of copper on the reduction percentage. The highest reduction percentage of copper was at 30 mg/L at optimal condition of nanocomposite bentonite/PVA-PVP/Fe_XO_y in previous data. At 30 mg/L, the value of removal percentage minimized because of diminishing the active core functional groups on nanocomposite bentonite/PVA-PVP/Fe_XO_y on the outer surface. It might be the nanocomposite pores reached to super-saturation.

Illustrating the effect of varies iron concentrations on reduction percentage, the highest removal percentage value of iron ions was 50 mg/L at optimal condition of nanocomposite bentonite/PVA-PVP/Fe_XO_y before. After this value, the reduction percentage diminished. This is due to minimizing active site functional groups on nanocomposite bentonite/Fe_XO_y. The effect of manganese ions concentration on nanocomposite bentonite/PVA-PVP/Fe_XO_y was examined, where the active sites of nanocomposite surface reached to

supersaturation of polluted element and the reduction percentage decreased. At 30 mg/L, the reduction percentage of manganese was 85.66% and it was the highest value. After this value the reduction percentage decreased.

Table (8). Effect of different concentrations of synthesized polluted cobalt ion on reduction percentage at optimal conditions of nanocomposite.

	Synthetized Solution concentration (mg/L)		
Parameter	**Before treatment**	**After treatment**	**Reduction %**
Cobalt	10	2.45	75.50
	20	4.60	77.00
	30	6.23	79.23
	50	8.30	83.40
	60	14.90	75.10
Chromium	10	1.95	80.50
	20	3.25	83.75
	30	4.60	84.66
	50	9.54	80.92
	60	12.27	79.55
Copper	10	2.75	72.50
	20	3.19	84.05
	30	4.05	86.50
	50	10.10	79.80
	60	13.22	77.96
Iron	10	2.24	77.60
	30	5.40	82.00
	50	4.97	90.06
	70	8.35	88.07
	90	15.00	83.33
Manganese	10	3.12	68.80
	20	3.45	82.75
	30	4.30	85.66
	50	11.68	76.64
	60	14.02	76.63

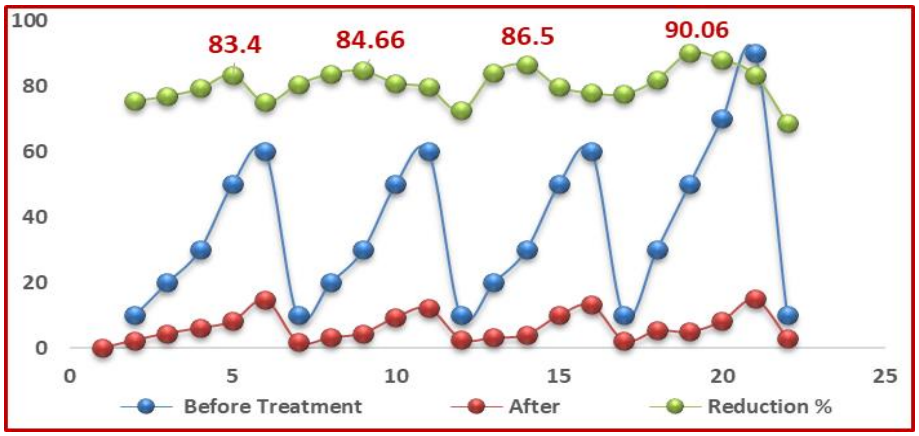

Fig. (13). Effect of removal efficiency of bentonite/PVA-PVP/Fe_xO_y nanocomposite on synthetized solution of Co, Cr, Cu, Fe and Mn.

6. Rehabilitation and Reusability of Adsorbents

Regeneration of nanocomposite adsorbents can reduce the estimation of technical operation of removing several pollutants. Wastewater treatment technologies are to get on materials that have a high adsorption rate without deterioration that might reduce the water pollution. Regeneration of the nanocomposite is the big important operation to check availability of nanocomposite sorption. In this paper, ten successive adsorption–desorption series operated. Reusability of pollutants adsorbed on Zeo. / Mon. /IONPs was done by 0.1 M HCl with rapid cleave at 180 rpm for 1 h at 25℃. The data performed by nanocomposite after ten adsorption–desorption series are shown in Table (9) and Fig. (14). The regeneration settlement was observed with procedures several times. The decreasing of sorption capacity after eight repeating cycles was shown. The synthesized nanocomposite could be good used for treating wastewater pollutants at least eight times.

Table (9). The relation between reusability cycles and different pollutants of nanocomposite Zeo. / Mon. /IONPs.

Pollutants	**Reusability cycles/Removal efficiency (%)**							
	1	**2**	**3**	**4**	**5**	**6**	**7**	**8**
Cobalt	83	80	68	64	62	61	60	58
Chromium	84	82	70	68	66	62	59	57
Copper	83	81	79	77	74	73	71	68
Iron	88	85	83	81	80	78	77	74
Manganese	91	88	86	84	82	80	78	75

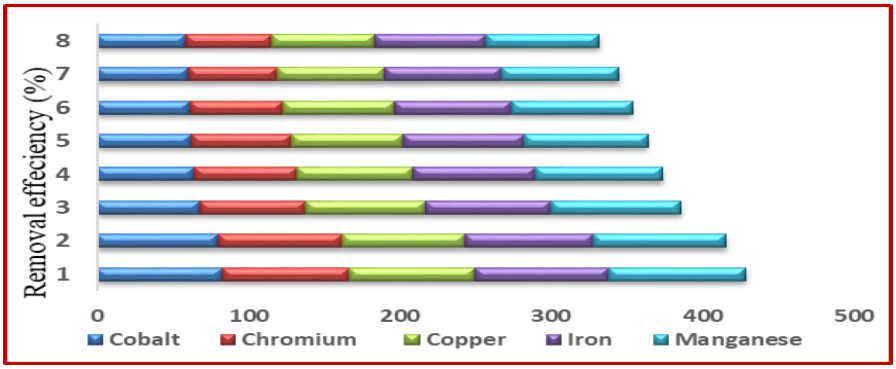

Fig. (14). Relation between reusability cycles/removal efficiency (%) of bentonite/PVA-PVP/Fe_xO_y nanocomposite on Co, Cr, Cu, Fe and Mn ions.

7. The Adsorption Isotherm and Balance Studies

The adsorption balance studies reflect the relation of the amount of adsorbate particle on the face of synthetized nano compound (Table 10 and Fig. 15, 16 and 17). Longmuir and Freundlich models are the mathematical equations that set the quantity of adsorbate. An adsorption investigation was donated to model of the influence of process variables for illuminate pollutants. Physical adsorption comes out from van der Waals forces between the adsorbate gas molecules and adsorbent face area (WHO, 2004).

Table (10). Parameters effect of both Langmuir and Freundlich models.

Pollutants	Langmuir isotherm				Freundlich isotherm			BET model		
	q_m (mg/g)	K_L	R_L	R^2	1/n	K_f	R^2	R^2	A	$X_{m(mg/g)}$
Cobalt	-68.0272	-130.839	-6540.96	0.83704	0.29517	0.486316	0.8668	0.926	37.50	0.33
Chromium	-274.725275	-1253.88	-62693	0.7227	0.49386	0.133158	0.9691	0.985	75.24	0.85
Copper	-104.166667	-374.93	-18745.5	0.89503	0.59506	0.156599	0.916	0.993	42.31	0.66
Iron	-117.647059	-258.753	-12936.6	0.8256	0.57173	0.20231	0.9471	0.970	52.10	0.58
Manganese	-120.192308	-395.148	-19756.4	0.8785	0.56067	0.178336	0.9149	0.960	55.47	0.88

qe (mg g^{-1}) is the adsorbed quantity of Fe and Mn ions at equilibrium per unit mass of magnetic nanocomposite, Ce (mg L^{-1}) is equilibrium concentration, q_m (mg/g^{-1}) theoretical adsorption capacity, K_L is Langmuir constant, K_F and n are Freundlich constants, $X_{m\ (mg/g)}$ (amount of adsorbate adsorbed by the coagulant to form a monolayer), *A* (interaction energy between adsorbate and coagulant surface), correlation coefficients (R^2).

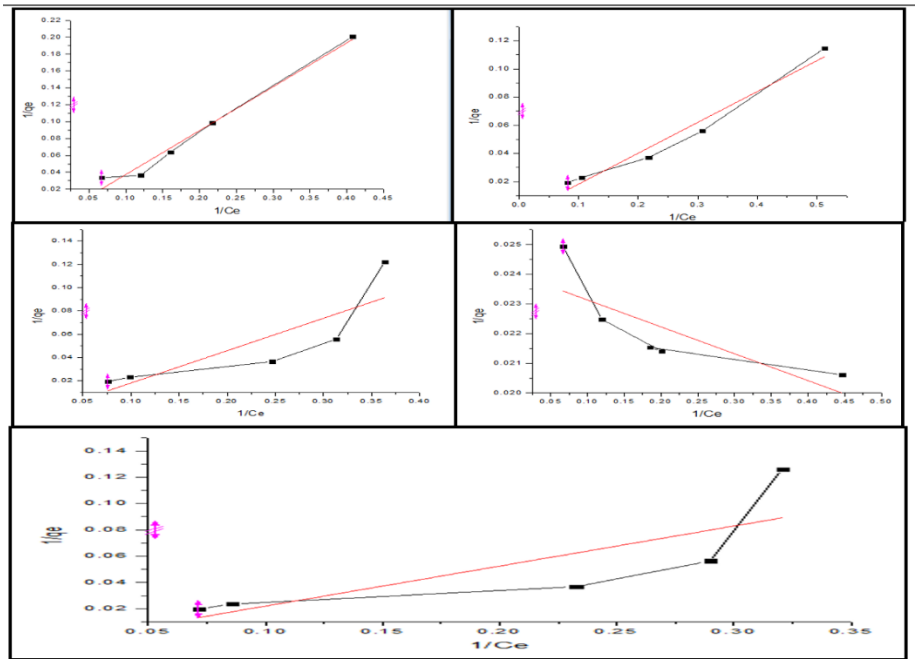

Fig. (15). Langmuir isotherm modeling for removes of Co, Cr, Cu, Fe and Mn by bentonite/PVA-PVP/Fe_xO_y nanocomposite.

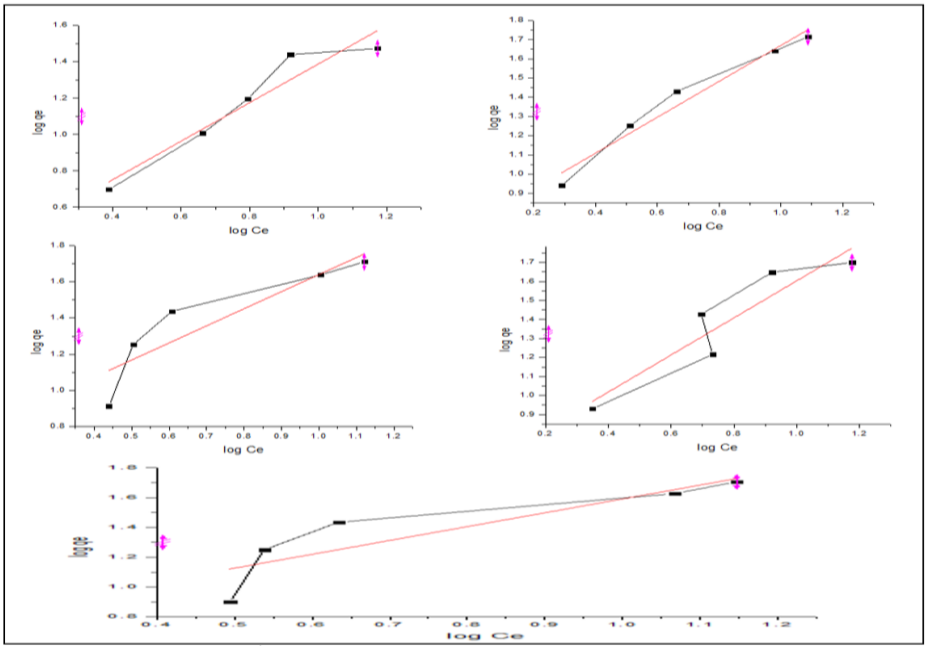

Fig. (16). Frendlish isotherm model for the remove of Co, Cr, Cu, Fe and Mn ions bentonite/PVA-PVP/Fe_xO_y nanocomposite.

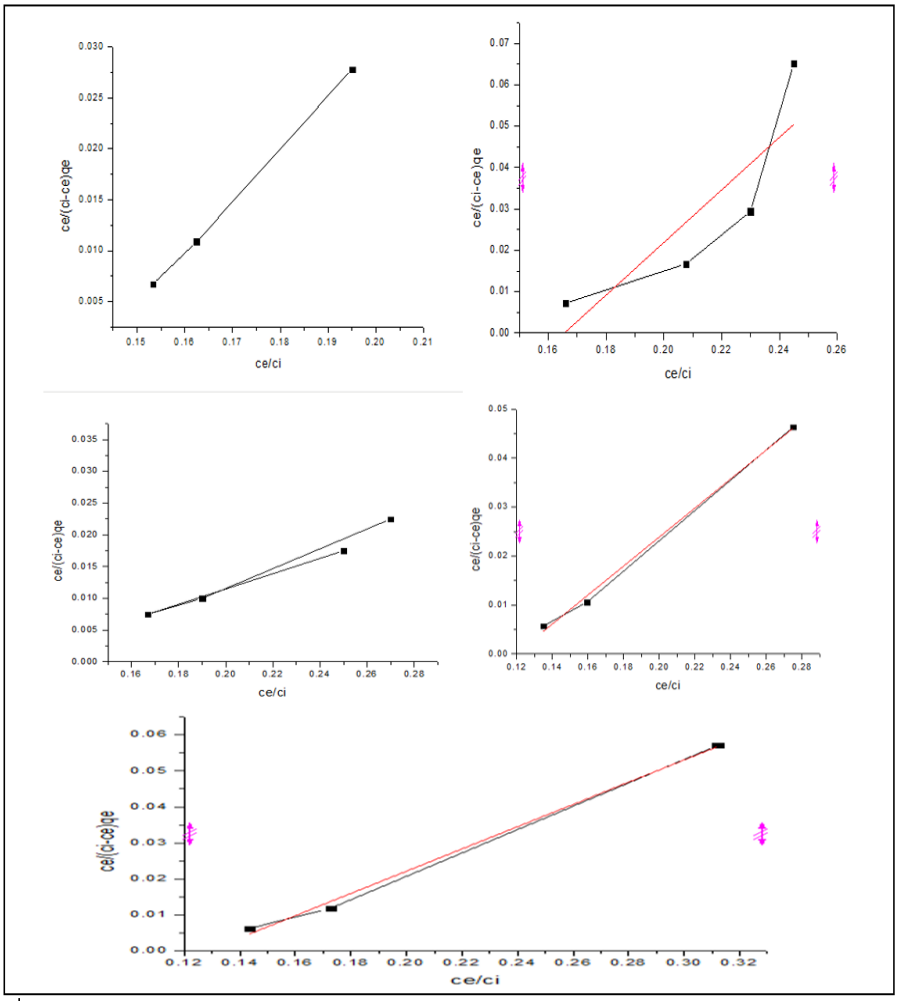

Fig. (17). BET isotherm model for the remove of Co, Cr, Cu, Fe and Mn ions bentonite/PVA-PVP/Fe_xO_y nanocomposite.

8. Effect of Temperature and Adsorption Thermodynamics and Kinetics

In this research, adsorption experiments were performed at different temperatures and optimal condition of nanocomposite dosage at certain pH (Singh et al., 2011). The temperature relines of C_e and q_e are shown in Table (11) and Fig. (18). As the temperature increased from 30 to 80°C, the pollutant induction rate weakly increased. This indicated that the adsorption power of nanocomposite was favored at high temperature, which proposed that the adsorption called endothermic. Moreover, thermodynamic analysis showed the occurrence of chemisorption which increased with increasing temperature.

This was because of the concomitant facilitation of diffusion (Daou et al., 2017).

Table (11). Thermodynamic parameters for different pollutants sorption on the adsorbent.

	Pollutants	Temp. (K)	K_L	ΔG^0 (KJ.mole^{-1})	ΔH^0 (KJ.mole^{-1})	ΔS^0 (KJ.mole^{-1})	R^2
Adsorbent	Cobalt	313	10.3922	-6.0920	6.190272	-0.23545	0.96744
		323	8.5604	-5.7660			
		333	9.2777	-6.1672			
		343	11.122	-6.8696			
		353	7.9272	-6.0760			
	Chromium	313	8.713	-5.6334	6.578057	-2.21934	0.99921
		323	8.8830	-5.8653			
		333	8.2207	-5.8324			
		343	9.6051	-6.4514			
		353	7.2085	-5.7971			
	Copper	313	7.5787	-5.2705	6.035264	0.118225	0.85002
		323	9.4182	-6.0224			
		333	9.7596	-6.3074			
		343	10.196	-6.6217			
		353	7.7221	-5.9990			
	Iron	313	9.6836	-5.9083	3.849201	6.716797	0.89373
		323	9.4459	-6.0303			
		333	9.6810	-6.2851			
		343	11.263	-6.9054			
		353	8.1331	-6.1512			
	Manganese	313	10.180	-6.0385	9.136309	-7.382	0.93119
		323	12.056	-6.6856			
		333	11.509	-6.7640			
		343	11.747	-7.0255			
		353	9.0619	-6.4686			

where K_L is the distribution coefficient, q_e (mg.g^{-1}) is the uptake capacity at equilibrium and C_e (mg.L^{-1}) is the equilibrium concentration of the adsorbate and ΔG^o (kJ mol^{-1}) is the change in Gibb's free energy, ΔS^o (J/mol K^{-1}) is the change in standard entropy, ΔH^o (KJ/mol) is the change in standard enthalpy, T (K^0) is the kelvin temperature and R (8.314 J mol^{-1} K^{-1}) is the general gas constant.

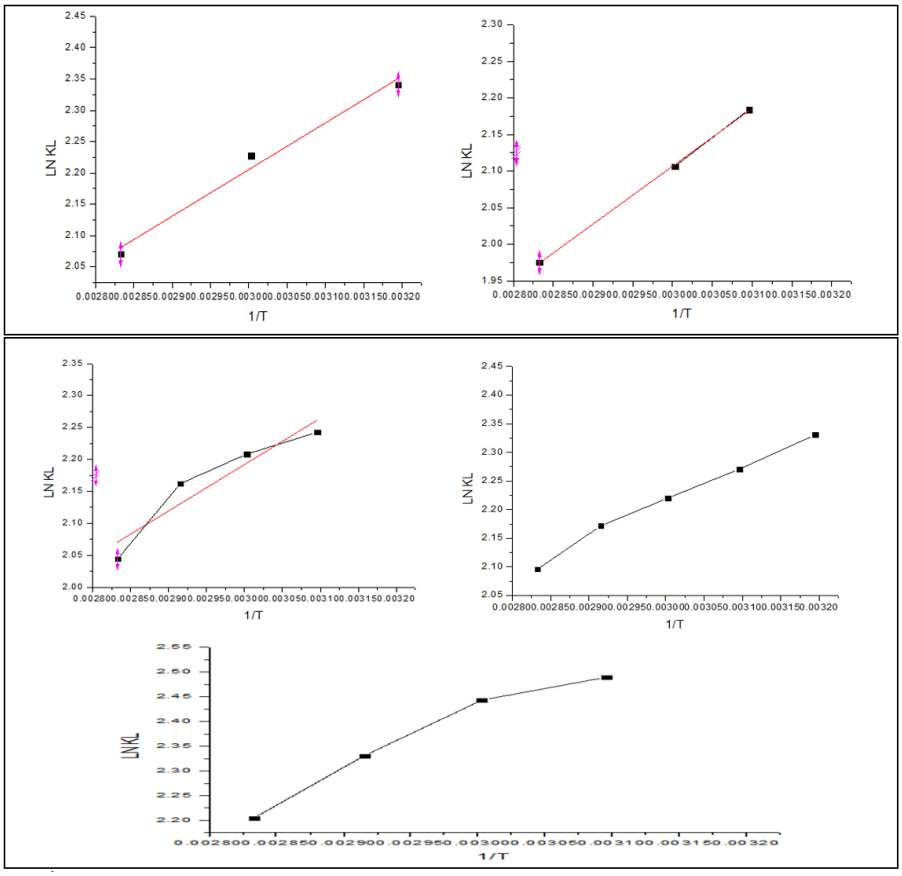

Fig. (18). Thermodynamic curves for different pollutants sorption onto nanocomposite adsorbent (trick of ln K_L x 1/T).

The temperature of reaction had less effect on the induction rate. The effect of temperature on adsorption was studied by thermodynamic analysis using Eqn. (12) – (15) to determine changes in the Gibbs free energy (ΔG), enthalpy (ΔH), and entropy (ΔS): (Anoop Krishnan and Anirudhan, 2002 and Chen et al., 2018).

$$K_L = qe / Ce \quad (1)$$

$$Ln\ K_L = \Delta S/ R - \Delta H/ RT \quad (2)$$

$$\Delta G = \Delta H - T\Delta S \quad (3)$$

$$\Delta G = - RT \ln K_L \quad (4)$$

Where K_L is adsorption distribution constant (L/g). ΔH and ΔS were getting by plot of ln K_L vs. 1/T which gives for the set of ΔG. Table (11) shows

thermodynamic parameters and calculated correlated coefficients and shows ΔH in positive value. This indicated that the nanocomposite adsorption was endothermic. The positive value of ΔS proposed that adsorption rose at the solid–liquid interface. Increasing temperature affect the negativity of ΔG values. Furthermore, the increase in ΔG with increasing temperature suggested that the adsorption on nanocomposite was more valuable at high temperatures. Negative value of Gibb's free energy shows the thermodynamic content and sorption process. The positive value of ΔH^o confirmed the endothermic nature of iron sorption. Positive value of enthalpy indicated the increase at the solid solution interface during the fixation of adsorbates on the active places of adsorbent. The effect of nanocomposite particle size on the Fe and Mn adsorption percentage showed that the adsorption rate for ions increased with decreasing particle size of nanocomposite.

9. Adsorption Capacities Comparison of Different Pollutants Obtained by Different Adsorbents

The observed adsorption capacity of for the removal of bentonite/PVA-PVP/Fe_xO_y nanocomposite on Co, Cr, Cu, Fe and Mn ions is acceptable when compared to that obtained by different adsorbents (Table 12).

Table (12). Adsorption capacities comparison of different pollutants obtained by varied materials.

Adsorbent	**Adsorption capability (mg/g)**	**References**
Magnetic bentonite (M-B) Fe3O4	26.18	Zou et al. (2018)
Raw Bentonite	63.70	Zuzana (2017)
Magnetic Bentonite	76.90	Zuzana (2017)
Hydroxyapatite-sodium alginate	142.85	Shabani et al. (2019)
Hydroxyapatite-sodium	77.51	Shabani et al. (2019)
Magnetic Iron/Bentonite Nanoparticles	6.33	Hao et al. (2009)
Nanocomposite of bentonite/PVA-PVP/Fe_xO_y Cobalt	68.02	
Nanocomposite of bentonite/PVA-PVP/Fe_xO_y Chromium	274.72	
Nanocomposite of bentonite/PVA-PVP/Fe_xO_y Copper	104.16	
Nanocomposite of bentonite/PVA-PVP/Fe_xO_y Iron	117.64	
Nanocomposite of bentonite/PVA-PVP/Fe_xO_y Manganese	120.19	Present work

CONCLUSION

In this paper, the adsorption technology was done and showed the relation between adsorbate materials and adsorbent in solution. Bentonite had different structures in tetragonal and octagonal shapes. The X-ray analysis explained SiO_2 and Al_2O_3 as main components of natural bentonite. These shapes depend mainly on Si-O and Al-O bonds, these bonds gave more active sites on oxygen atoms and hydroxyl groups. The bentonite clay mineral had a definite structure which depends on varies crystallographic shapes the chemical crystallographic shapes (tetragonal and octagonal shapes). Also, a new methodology for purification of clay minerals with high quality and lowest cost was represented. Using iron nanoparticles in our study with nanocomposite gave high removable percentage values of heavy metals in wastewater samples. The grafting copolymerization process occurred with bentonite shapes and a mixture hydrolysate of PVA and PVP as cross-linking polymerization binder. Bentonite/PVA-PVP/FexOy was investigated by different characterization analyses such as XRD, FT-IR, SEM, particle size distribution and VSM. We were gotten on a new nanocomposite which contained on supported treated minerals (hydrolosate bentonite/PVA-PVP) coated with several millions of negative oxygenated attached to nano-Fe_XOy as a core ions. The average of nanocomposite formed by SEM images illustrate that magnetite was intersected through the inside bentonite and average diameter size was 14.5-31.50 nm. Optimal conditions of nanocomposite dosage were 7.5 g/L and touch time 30 min at 50^{o}C and pH solution 6.0. Bentonite/PVA-PVP/Fe_XO_y adsorbent considered as an excellent adsorbent at lower pH. Adsorption rate included static interaction between functional groups of bentonite/PVA-PVP/Fe_XO_y surface and negative groups of heavy metals. This paper focused on the nature of bentonite/PVA-PVP/Fe_xO_y for removing pollutants. The removal efficiency of five heavy metals (Co, Cr, Cu, Fe, and Mn) was 83.40%, 84.66%, 86.50%, 90.06% and 85.66%. Optimal conditions of nanocomposite bentonite/PVA-PVP/Fe_XO_y experiment were nanocomposite dosage at 7.5 g/L; contact time at 30 min; temperature at 50^{o}C and pH at 6.0.

Novelty Statement

Recently, the mixing of magnetic iron nanoparticles with bentonite mineral with PVA/PVP solution formed new composite bentonite/PVA-PVP/Fe_xO_y. The purification steps of local Egyptian clay minerals were carried out by a simple methodology and low cost. This new composite as adsorbents has high reduction percentage of different heavy metals in wastewater treatment. The new composite bentonite/PVA-PVP/Fe_xO_y can increase the mechanical strength of adsorbents and develop the different application of nano-magnetic composite in wastewater treatment. The

prepared new composite bentonite/PVA-PVP/Fe_xO_y was used in the removal of five heavy metals ions in samples from wastewater and showed high adsorption efficiency percentage.

REFERENCES

Abbas, M., M. Takahashi and C. Kim (2013). Facile sonochemical synthesis of high-moment magnetite (Fe_3O_4) nanocube. J. Nanopart. Res., 15: 1354.

Adriane, K., J. Huang, G. Ding, J. Chen and Y. Liu (2006). Self-assembled magnetic PVP/PVA hydrogel microspheres; magnetic drug targeting of VX2 auricular tumors using pingyangmycin. J. Drug Target, 14: 243-253.

Anoop Krishnan, K. and T.S. Anirudhan (2002). Removal of mercury (II) from aqueous solutions and chlor-alkali industry effluent by steam activated and sulphurised activated carbons prepared from bagasse pith. J. Hazard. Mater., 92: 161–183.

Betega, d.L., A.R. Morales and F.R. Valenzuela Diaz (2008). Organo clays properties, preparation and applications. Appl. Clay Sci., 42: 8-24.

Bourlinos, A.B., M.A. Karakassides, A. Simopoulos and D. Petridis (2000). Synthesis and characterization of magnetically modified clay composites. Chem. Mater., 12: 2640–2645.

Brazel, C.S. (2009). Magneto-thermally-responsive nanomaterials: Combining magnetic nanostructures and thermally-sensitive polymers for triggered drug release. Pharm. Res., 26: 644–656.

Catalano, E., M. Miola, S. Ferraris, S. Novak, F. Oltolina, A. Cochis, M. Prat, E. Vernè, L. Rimondini and A. Follenzi (2017). Magnetite and silica-coated magnetite nanoparticles are highly biocompatible on endothelial cells *in vitro*. Biomed. Phys. Eng. Express, 3: 025015.

Chen, Q.S., B. Huang, S.W. Wang and L.Y. Wang (2018). Adsorption behavior of magnetic bentonite for removing Hg(II) from aqueous solutions J. Radioanal. Nucl. Chem., 316: 71-80.

Choe, S., Y.Y. Chang, K.Y. Hwang and J. Khim (2000). Kinetics of reductive denitrification by nanoscale zero-valent iron. Chemosphere, 41 (8): 1307-1311.

Cornell, R.M. and U. Schwertmann (2003). In: 'Iron Oxides'. 2nd Ed., Wiley-VCH Verlagsgesellschaft Weinheim

Daou, O. Zegaoui and A. Amachrouq (2017). Study of the effect of an acid treatment of a natural Moroccan bentonite on its physicochemical and adsorption properties. Water Sci. Technol., 75: 1098–1117.

De Mello, K.K.L.B., L.C. Varanda, F.A. Sigoli and I.O. Mazali (2019). Co-precipitation synthesis of (Zn-Mn)-codoped magnetite nanoparticles and their application in magnetic hyperthermia. J. Alloys Compd., 11: 698–705.

Gonzalez, J.S., P. Nicolás, M.L. Ferreira, M. Avena, V.L. Lassalle and V.A. Alvarez (2014). Fabrication of ferrogels using different magnetic nanoparticles and their performance on protein adsorption. Polym. Int., 63 (2): 232.

Guo, L., G. Liu, R.Y. Hong and H.Z. Li (2010). Preparation and characterization of chitosan poly (acrylic acid) magnetic microspheres. Marine Drugs, 8: 2212–2222.

Hao, J., M.J. Han and X. Meng (2009). Preparation and evaluation of thiol-functionalized activated alumina for arsenite removal from water. J. Hazard Mater., 167: 1215-1221.

He, H., Y. Ma, J. Zhu, P. Yuan and Y. Qing (2010). Organo clays prepared from montmorillonites with different cation exchange capacity and surfactant configuration. Appl. Clay Sci., 48 (1–2): 67–72.

Hidayat, M.F., S. Sunaryono, N. Mufti and E. Latifah (2019). Study on distribution of magnetite (Fe_3-xMnxO_4) filler in Fe3-xMnxO4-PEG/PVA/PVP magnetic hydrogel by using two lognormal function analysis. IOP Conf. Ser., Mater. Sci. Eng., p. 515.

Hong, R.Y., S.Z. Zhang, Y.P. Han, H.Z. Li, J. Ding and Y. Zheng (2006). Preparation, characterization and application of bilayer surfactant stabilized ferro-fluids. Powder Technology, 170: 1-11.

Huang, Y.H. and T.C. Zhang (2002). Kinetics of nitrate reduction by iron at near neutral pH. Journal of Environmental Engineering, 128 (7): 604-611.

Indira, T.K. and P.K. Lakshmi (2010). Magnetic nanoparticles - A review. Int. J. Pharm. Sci. Nano-Technol., 3: 1035-1042.

Karimzadeh, I., M. Aghazadeh, T. Doroudi, M.R. Ganjali and P.H. Kolivand (2017). Effective preparation, characterization and *in situ* surface coating of superparamagnetic Fe_3O_4 nanoparticles with polyethylene mine through cathodic electrochemical deposition (CED). Curr. Nanosci., 13: 167–174.

Karnland, O., S. Olsson and U. Nilsson (2006). Mineralogy and sealing properties of various bentonites and smectite-rich clay materials. Technical Report. SKB Stockholm.

Kurlyandskaya, G.V., A.V. Svalov, B.A. Burgoa, F.A. Blyakhman, A.P. Safronov, F.A. Blyakhman, A.V. Svalov, E. Fernández, E. Fernández, A.P. Safronov and I.V. Beketov (2017). Magnetoimpedance biosensor prototype for ferrogel detection. J. Magn. Mater., 441: 650-655.

Li, H., Z. Lu, G. Cheng, K.F. Rong, F.X. Chen and R. Chen (2015). HEPES-involved hydrothermal synthesis of Fe_3O_4 nanoparticles and their biological application. RSC Adv., 5: 5059–5067.

Lu, G., S. Li, Z. Guo, O.K. Farha, B.G. Hauser, X. Qi, Y. Wang, X. Wang, S. Han, X. Liu, J.S. Duchene, H. Zhang, Q. Zhang, X. Chen, J. Ma,

S.C.J. Loo, W.D. Wei, Y. Yang, J.T. Hupp and F. Huo (2012). Imparting functionality to a metal-organic framework material by controlled nanoparticle encapsulation. Nat. Chem., 4: 310–316.

Mahdavi, M., F. Namvar, M.B. Ahmad and R. Mohamad (2007). Green biosynthesis and characterization of magnetic iron oxide (Fe3O4) nanoparticles using seaweed (*Sargassum muticum*) aqueous extract. Moecules, 18: 5954–596.

Moise, S., E. Céspedes, D. Soukup, J.M. Byrne, A.J. El Haj and N.D. Telling (2017). The cellular magnetic response and biocompatibility of biogenic zinc- and cobalt-doped magnetite nanoparticles. Sci. Rep., 7: 1–11.

Morjan, I., R. Alexandrescu, F. Dumitrache, R. Birjega, C. Fleaca, I. Soare, C.R. Luculescu, G. Filoti, V. Kuncer and L. Vekas (2010). Iron oxide-based nanoparticles with different mean sizes obtained by the laser pyrolysis: structural and magnetic properties. J. Nanosci. Nanotechnol., 10: 1223–1234.

Murray, H.H. (2006). In: 'Applied Clay Mineralogy: Occurrences, Processing and Applications Of Kaolins, Bentonites, Palygorskitesepiolite, and Common Clays'. Vol 2. Elsevier, Amsterdam.

Okoli, C., M. Sanchez-Dominguez, M. Boutonnet, S. Järås, C. Civera, C. Solans and G.R. Kuttuva (2012). Comparison and functionalization study of microemulsion-prepared magnetic iron oxide nanoparticles. Langmuir., 28: 8479–8485.

Ooi, F., J.S. DuChene, J.J. Qiu, J.O. Graham, M.H. Engelhard, G.X. Cao, Z. Gai and W.D. Wei (2015). A facile solvothermal synthesis of octahedral fe3o4 nanoparticles. Small, 11: 2649–2653.

Petcharoen, K. and A. Sirivat (2012). Synthesis and characterization of magnetite nanoparticles via the chemical co-precipitation method. Mater. Sci. Eng. B-Adv., 177: 421–427.

Safronov, A.P., E.A. Mikhnevich, Z. Lotfollahi, F.A. Blyakhman, T.F. Sklyar, A. Larrañaga Varga, A.I. Medvedev, S. Fernández Armas and G.V. Kurlyandskaya (2018). Polyacrylamide ferrogels with magnetite or strontium hexaferrite: Next step in the development of soft biomimetic matter for biosensor applications. Sensors, 18 (1): 257.

Shabani, E., F. Salimi and A. Jahangiri (2019). Removal of arsenic and copper from water solution using magnetic iron/bentonite nanoparticles (Fe_3O_4/bentonite). Silicon, 11: 961–971.

Shalaby, N., R. Elsalamony and A.M.A. El Naggar (2018). Mesoporous waste extracted SiO_2-Al_2O_3 supported Ni and Ni-H3PW12O40 nano-catalysts for photo-degradation of methyl orange dye under UV irradiation. New Journal of Chemistry, 42 (1) DOI: 10.1039/C8NJ01479E.

Sharma, G. and P. Jeevanandam (2013). Synthesis of self-assembled prismatic iron oxide nanoparticles by a novel thermal decomposition route., RSC Adv., 3: 189-200.

Shi, Y., D.S. Xiong, Y. Peng and N. Wang (2016). Effects of polymerization degree on recovery behavior of PVA/PVP hydrogels as potential articular cartilage prosthesis after fatigue test. Express Polym. Lett., https://doi.org/10.1063/5.0000890.

Singh, S., K.C. Barick and D. Bahadur (2011). Surface engineered magnetic nanoparticles for removal of toxic metal ions and bacterial pathogens. J. Hazard. Mater., 192:1539– 1547.

Solano, E., L. Perez-Mirabet, F. Martinez-Julian, R. Guzman, J. Arbiol, T. Puig, X. Obradors, R. Yanez, A. Pomar and S. Ricart (2012). Facile and efficient one-pot solvothermal and microwave-assisted synthesis of stable colloidal solutions of MFe_2O_4 spinel magnetic nanoparticles. J. Nanopart. Res., 14: 15.

Strobel, R. and S.E. Pratsinis (2007). Flame aerosol synthesis of smart nanostructured materials. J. Mater. Chem., 17: 4743–4756.

Sunaryono, H.M.F., C. Insjaf, A. Taufiq, N. Mufti and Munasir (2018). Investigation of magnetic properties and mechanical responses on hydrogel-TMAH-magnetite, IOP Conference Series: Materials Science and Engineering, 367 (1): 012025.

Sunaryono, T.A., E.G.R. Putra, A. Okazawa, I. Watanabe, N. Kojima, S. Rugmai, S. Soontaranon, Zainuri, S. Pratapa and Darminto (2016). Small-angle x-ray scattering study on PVA/Fe_3O_4 magnetic hydrogels, Nano 11: 1650027.

Tsukasa, T. (2017). Nanostructure engineering of size-quantized semiconductor particles for photo electrochemical. Electrochemistry, 85 (9): 534-542.

Wang, J.H., M.X. Gao, D.S. Wang, X. Li, Y.B. Dou, Y.F. Liu and H.G. Pan (2015). Chemical vapor deposition prepared bi-morphological carbon-coated Fe_3O_4 composites as anode materials for lithium-ion batteries. Power Sources, 282: 257–264.

Wisotzki, E.I., D. Eberbeck, H. Kratz and S.G. Mayr (2016). Magnetic response of gelatin ferrogels across the sol-gel transition: The influence of high energy crosslinking on thermal stability. Soft Matter, 12: 3908-3918.

WHO, World Health Organization (2004). Manganese and its Compounds: Environmental Aspects: Concise International Chemical Assessment Document. World Health Organization, Geneva, Switzerland.

Zhang, J., Q. Huang and J. Du (2016). Recent advances in magnetic hydrogels. Polym. Int., 65: 1365-1372.

Zou, C., J. Liang., W. Jiang., Y. Guan and Y. Zhang (2018). Adsorption behavior of magnetic bentonite for removing Hg (II) from aqueous solutions. RSC Advanced, 48: 27016-27595.

Zustiak, S.P. and J.B. Leach (2010). Hydrolytically degradable poly (ethylene glycol) hydrogel scaffolds with tunable degradation and mechanical properties. Biomacromolecules, 11: 1348-1357.

Zuzana, D., F. Erika, Bekényiová, Alexandra, Dankanova, Z. et al. (2017). Bentonite/iron. Archives for Technical Sciences 16 (1): 65-75.

كفاءة إزالة العناصر الثقيلة الملوثة لمياه الصرف باستخدام متراكب البوليمر النانوي لمعدن البينتونيت والمطعم بجزيئات عديد الفينيل الكحولى وعديد الفيدون والمجناتيت المغناطيسي

ياسر عبد المطلب عبد الهادي
وحده التلوث البيئي، قسم الهيدروجيوكيمياء، شعبة مصادر المياه والأراضي الصحراوية، مركز بحوث الصحراء، القاهرة، مصر

يهدف البحث إلى إستخدام تكنولوجيا النانو المغناطيسية لمركبات الحديد النانوية المجناتيت (FexOy) والمطعمة بأيونات عديد الفينيل الكحولى (PVA) وعديد الفيدون (PVP) ذات الطبيعة البولمرية الخاصة في إزالة الملوثات الأيونية لخمس عناصر ملوثة لمياه الصرف وذلك باستخدام مركب طبيعي لمعدن البينتونيت رخيص الثمن ومحلي الإنتاج في نموذج بحجم النانو باستخدام عملية الترسيب الكيميائى. تم فحص المركب النانوي الناتج باستخدام أجهزة فحص خواص المواد XRD وFT-IR وSEM وتوزيع حجم الجسيمات وكذلك جهاز VSM لقياس الخواص المغناطيسية للمركب الحديد النانوي الجديد. تم خلط جسيمات الحديد النانوية المغناطيسية مع معدن البنتونيت مع محلول PVA/PVP لتشكيل مركب بنتونايت جديد / FexOy / PVA-PVP. تم اتباع خطوات تنقية معادن الطين المصري المحلي بمنهجية بسيطة وبتكلفة منخفضة. يحتوي هذا المركب الجديد كمواد ماصة على نسبة اختزال عالية من المعادن الثقيلة المختلفة في معالجة مياه الصرف وكذلك يمكن للبنتونايت المركب الجديد / FexOy / PVA-PVP زيادة القوة الميكانيكية للمواد الماصة وتطوير التطبيقات المختلفة للمركب المغناطيسي النانوي في معالجة مياه الصرف. وقد أظهرت النتائج المعملية أن متوسط قطر أطوال المادة النانوية الجديدة حوالي ٣١.٥ نانومتر. من خلال القياسات المغناطيسية باستخدام VSMأظهرت نتائج التحليل الطبيعة المغناطيسية الفائقة للمركب النانوي. وقد أوضحت النتائج المعملية للبحث على ارتفاع معدلات إزالة المعادن الملوثة للمياه من خلال قدرة المركب النانوي الجديد على امتصاص وادمصاص الأيونات الملوثة الخمسة (Fe/Cu/Cr/Co/Mn) في التشابك البلوري البولمري الجديد وكانت نسب الإزالة كالتالي بالترتيب: ٨٣.٤٪، ٨٤.٦٦٪، ٨٦.٥٪، ٩٠.٠٦٪ و٨٥.٦٦٪) تحت الظروف المثلى للتجربة.